International Journal of Automotive Technology, Vol. 22, No. 1, pp. 173–184 (2021)
DOI 10.1007/s12239–021–0018–2

pISSN 1229–9138/ eISSN 1976–3832

EMERGENCY COLLISION AVOIDANCE BY STEERING IN CRITICAL SITUATIONS

Janghee Park, Dongchan Kim and Kunsoo Huh*

Department of Automotive Engineering, Hanyang University, Seoul 04763, Korea

(Received 16 January 2020; Revised 17 April 2020; Accepted 17 April 2020)

ABSTRACT–In this paper, an emergency collision avoidance system is proposed by including not only braking but also steering control actions. The minimum distance to avoid collision is calculated separately for braking and steering based on the relative motion to the surrounding vehicles and the lane information obtained through the vision sensor. For steering avoidance control, an optimal control input is calculated through the model predictive control that satisfies constraints such as safe avoidance region created by surrounding vehicles and capacity of the vehicle actuator. In particular, for avoiding collision by lane changing, the maximum lateral acceleration and the maximum angle of the trajectory are considered. In addition, the abrupt lateral movement in avoidance causes nonlinear characteristics in tires and, thus, tire parameters are estimated through EKF (Extended Kalman Filter) to improve model prediction accuracy. The control intervention time of avoidance maneuvering is determined for braking and steering, respectively. The simulation results demonstrate that the proposed algorithm of integrating AEB (Autonomous Emergency Braking) and AES (Autonomous Emergency Steering) can effectively avoid the collision in critical situations and that the host vehicle can still maintain the safety inside the road boundary.

KEY WORDS : Collision avoidance, AEB, AES, MPC

1. INTRODUCTION

Active safety system in vehicle can perform collision avoidance or damage mitigation control through the acquired information from vehicle internal states and in-vehicle sensors for the surroundings. The collision avoidance by braking is called AEB (Autonomous Emergency Braking), whereas collision avoidance by steering is called AES (Autonomous Emergency Steering).

The safety regulations such as Euro-NCAP (Schram *et al.,* 2013). promote the AEB technology as a safety feature and it has been installed in the mass-produced vehicles to avoid imminent collision. For the case of AES, there are few commercially available products yet, but many OEMs and suppliers have been developing the application of the AES for ADAS (Advanced Driver Assist Systems) and Autonomous Driving (Goodrich, 2013). In addition, because the Euro-NCAP 2020 ROADMAP (Euro NCAP, 2015) is referring the AES performance evaluation for certain collision scenarios, AES technology combined with the AEB is expected to be installed on mass-produced vehicles. Nonetheless, most collision avoidance researches have studied AEB or AES independently. When the host vehicle is confronted with complicated traffic situations with surrounding vehicles, the activation conditions for the AEB and AES may conflict to each other in emergency cases. Even if the upper-level judgment rules are needed for the effective collision avoidance, integration of the AEB and AES has not been actively investigated in the related literature.

In this paper, the AES system is designed for the emergency collision avoidance and its activation rules are proposed such that the AES is effective in situations where collision avoidance is impossible with the AEB. In order to predict the trajectory of the surrounding vehicles, vehicle shape is described as an ellipse considering the sensor characteristics and constant velocity is assumed during the time step. The prediction model for the host vehicle is improved in accuracy by considering the nonlinear characteristics of the tires during evasive steering. The variation of the cornering stiffness is estimated through EKF (Extended Kalman Filter) using the nonlinear vehicle dynamics model.

For the design of the AES system, the cost function is formulated including the tracking error and input size, where the target output consists of the desired lateral distance and heading angle for collision avoidance. Besides, safe avoidance region and actuator capacity are considered as constraints for the MPC design. In order to design the activation rules for the AES system, not only the TTC index, but also the maximum lateral acceleration

*Corresponding author. e-mail: khuh2@hanyang.ac.kr

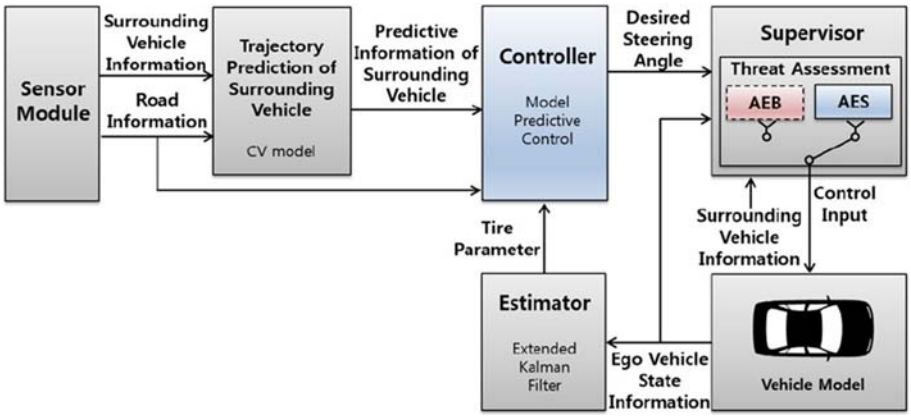

Figure 1. Overall system architecture.

index are proposed considering how steep the avoidance trajectory is for the host vehicle. The proposed AES system is evaluated in simulations and compared with the AEB for various collision scenarios. The simulation results demonstrate that the proposed AES system can effectively avoid the collision in critical situations which cannot be avoided by the conventional AEB. In addition, the simulation results show that the host vehicle can maintain the lane keeping safely inside the road boundary after the collision avoidance.

Figure 1 shows the overall structure of the proposed control system. Section 2 describes background of this study. In Section 3, methods of predicting the trajectory are explained for surrounding and host vehicles. Section 4 describes the MPC design with the objective function and the constraints. Section 5 explains the activation method for the AES as well as AEB for the effective collision avoidance. Section 6 presents simulation results for the proposed system.

2. BACKGROUND

AEB (Autonomous Emergency Braking) system is one of the most efficient way to lower social cost of traffic accidents. But, it should be noted that there exist certain imminent collisions which cannot be avoided by current AEB systems. By adding AES systems, some of those rear-end collisions can be avoided by evasive maneuvering at high speed (Eckert *et al.,* 2011). Because there are advantages and disadvantages of the AEB and AES systems depending on the relative motion with the surrounding vehicles, it is necessary to determine the collision risk and intervention time for AEB and AES systems, respectively.

In the previous studies of AEB, the most commonly used method is to calculate the collision risk by TTC (Time-To-Collision) when braking is applied (Shah and Benmimoum, 2015; Tamke *et al.,* 2011; Berthelot *et al.,* 2012). The smallest TTC for AEB activation can be obtained assuming that the longitudinal deceleration of the vehicle is constant. Otherwise, the stopping distance (Lee *et al.,* 2014) is also utilized for the activation when the deceleration varies during the AEB operation. Similarly, in the case of AES, the most commonly used method is to calculate the smallest TTC for AES activation. In particular, when calculating the TTC for the AES, the lateral acceleration is typically assumed constant during the lateral avoidance. Because the AES should include the steering actions for both avoiding the collision and keeping the lane, the collision avoidance based on the constant acceleration only does not guarantee that the entire avoidance path is safe and feasible.

In case of determining when to activate emergency control, finding the last possible evasive trajectory method (Schmidt *et al.,* 2006; Söntges and Althoff, 2015) was studied. All the collision-free trajectories are calculated considering longitudinal and lateral motions. The intervention time is determined as the last possible point for the existence of evasive trajectory. However, these methods cannot be easily applied for integrated ADAS functions where AEB and AES operate separately with independent ECUs.

From the steering control perspectives for AES, optimal input design based on the MPC (Model Predictive Control) scheme has been extensively studied by using the predicted path (Falcone *et al.*, 2007; Yoon *et al*., 2009; Liu *et al*., 2017; Carvalho *et al*., 2014; Werling and Liccardo, 2012). An optimal tracking problem with a nonlinear vehicle model was studied under stability constraints (Falcone *et al.*, 2007; Yoon et al., 2009). MPC framework with an extensive cost function (Liu et al., 2017; Carvalho et al., 2014; Werling and Liccardo, 2012) was also designed including trajectory error, lane selection and change, and risk index. After optimal paths are generated based on the index, they are realized by combination of accelerating, braking and steering. Driver incompatibility was considered by Kim et al (Kim *et al.,* 2017) where MPCs are separately formulated for possible braking, moving left and right and the optimal input is selected among the avoidance paths. In order to design steering controllers for collision avoidance, an environmental envelope (Erlien *et al.,* 2016) was described as a boundary line for static obstacles and the

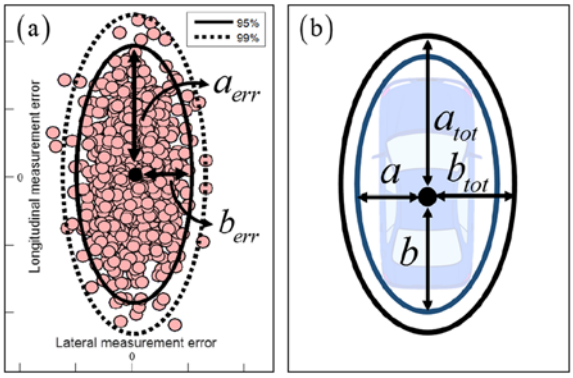

Figure 2. Vehicle shape representation: (a) error ellipse and (b) boundary of vehicle.

safe avoidance region was determined. Safety bubble (Keller *et al.,* 2015) was used to define the risk region of the surrounding vehicles and the collision avoidance control is performed when the host vehicle enters the safety bubble. Even if various cost functions were designed for MPC based collision avoidance, the different characteristics of collision avoidance using braking and steering have not been well investigated.

3. TRAJECTORY PREDICTION OF VEHICLES

When the collision is expected, the safe avoidance region can be defined based on the predicted trajectories of the surrounding vehicles and the host vehicle. In this study, vehicle shape is represented as an ellipse whose size is determined by the sensor characteristics. If the measurement error of the sensors mounted on the vehicle is assumed to be a random variable, the standard deviation of the error is expressed as σ_x and σ_y in the longitudinal and lateral directions, respectively. Based on the constant probability of δ, the size of the error ellipse can be geometrically illustrated into Figure 2 (a) and its parameters can be obtained from the following equations (Ribeiro, 2004).

$$K = -2\ln(\delta) \tag{1}$$

$$a_{err} = \sigma_x \sqrt{K},\ \ b_{err} = \sigma_y \sqrt{K} \tag{2}$$

As shown in Figure 2 (a), the larger the probability is, the larger the size of the error ellipse is. For the conservative collision avoidance, the probability is set to a large value of 0.95 in this study. Then, the vehicle shape can be also expressed as a geometric ellipse as shown in Figure 2 (b) where the error size in equation (2) is added to the overall length and width of the surrounding vehicle, respectively.

$$\begin{aligned} a_{tot} &= a + a_{err} \\ b_{tot} &= b + b_{err} \end{aligned} \tag{3}$$

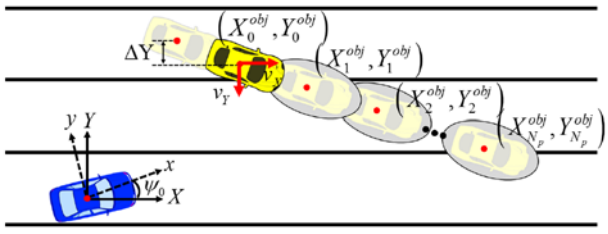

Figure 3. Predicted trajectory of the surrounding vehicle.

3.1. Trajectory Prediction of Surrounding Vehicles

In order to predict the trajectory of the surrounding vehicle, the global velocity of the host vehicle, relative distance and velocity to the surrounding vehicle and lane information are utilized. As illustrated in Figure 3, two coordinate systems are positioned at the center of the host vehicle. One is the vehicle coordinate system, x-y, and the other is the inertial coordinate system, X-Y. After the heading angle, ψ, is obtained from the lane information, the relative distance measured in the vehicle coordinate system can be converted into the position on the inertial coordinate system.

In order to predict the future position of the surrounding vehicle in the inertial coordinate system, the absolute velocities of the surrounding vehicle are calculated as follows.

$$\begin{aligned} v_X^{obj} &\cong v_x^{ego} + v_{x,rel} \\ v_Y^{obj} &= \Delta Y^{obj} / T_{sen} \end{aligned} \tag{4}$$

where v_X^{obj} and v_Y^{obj} are the velocity of the surrounding vehicle in X-direction and Y- direction, v_x^{ego} is the velocity of the host vehicle in x-direction, $v_{x,rel}$ is the relative velocity of the surrounding vehicle, ΔY^{obj} is the lateral distance of the surrounding vehicle during one sampling period and T_{sen} denotes sampling period of on-board sensors, respectively.

In the above formulation, v_x^{ego} is approximated as the velocity in the inertial coordinate mainly because the host vehicle is typically following the lane. Assuming that the velocities in equation (4) are constant over the prediction horizon (Lefèvre *et al.*, 2014), the future position of the surrounding vehicle can be predicted by equation (5).

$$\begin{aligned} X_{k+1}^{obj} &= X_k^{obj} + T_s \cdot v_X^{obj} \\ Y_{k+1}^{obj} &= Y_k^{obj} + T_s \cdot v_Y^{obj} \\ k &= 1, \cdots, N_p \end{aligned} \tag{5}$$

where X_k^{obj} and Y_k^{obj} are the position of the surrounding vehicle in X-direction and Y-direction for k step, N_p is the number of time steps for prediction horizon and T_s is the control time step, respectively.

In order to determine the safe avoidance region, the predicted vehicle position on the inertial coordinate system is converted back to the position on the vehicle coordinate system using the following equation.

$$\begin{bmatrix} x_k^{obj} \\ y_k^{obj} \end{bmatrix} = \begin{bmatrix} \cos\psi_o & \sin\psi_o \\ -\sin\psi_o & \cos\psi_o \end{bmatrix} \begin{bmatrix} X_k^{obj} \\ Y_k^{obj} \end{bmatrix} \tag{6}$$

where ψ_o is the heading angle of the vehicle.

3.2. Trajectory Prediction of the Host Vehicle

For the collision avoidance against the moving vehicles, it is also necessary to predict the states of the host vehicle over the prediction horizon. The bicycle model in Figure 4 is used to predict the lateral behavior of the host vehicle. Because the collision avoidance by steering involves severe cornering, nonlinear characteristics of tires should be considered for accurate prediction. Thus, time-varying cornering stiffness are assumed in equation (7).

$$\begin{aligned}\dot{\mathbf{x}}(t) &= A\mathbf{x}(t) + B\mathbf{u}(t)\\ \mathbf{y}(t) &= C\mathbf{x}(t)\end{aligned} \tag{7}$$

where $\mathbf{x} = \begin{bmatrix} y & \beta & \psi & \dot{\psi} \end{bmatrix}^T$, $\mathbf{u} = \delta_f$, $\mathbf{y} = \begin{bmatrix} y & \psi \end{bmatrix}^T$,

$$A = \begin{bmatrix} 0 & v_x & v_x & 0 \\ 0 & \dfrac{-2(C_f + C_r)}{mv_x} & 0 & -1 + \dfrac{-2(l_f C_f - l_r C_r)}{mv_x^2} \\ 0 & 0 & 0 & 1 \\ 0 & \dfrac{-2(l_f C_f - l_r C_r)}{I_z} & 0 & \dfrac{-2({l_f}^2 C_f + {l_r}^2 C_r)}{I_z v_x} \end{bmatrix},$$

$$B = \begin{bmatrix} 0 \\ \dfrac{2C_f}{mv_x} \\ 0 \\ \dfrac{2l_f C_f}{I_z} \end{bmatrix},\ C = \begin{bmatrix} 1 & 0 & 0 & 0 \\ 0 & 0 & 1 & 0 \end{bmatrix}.$$

where y, β, ψ, $\dot{\psi}$ and δ_f are, respectively, the vehicle lateral position, side-slip angle, yaw angle, yaw rate and front wheel steering angle. C_f and C_r are the front and rear cornering stiffness. v_x, m and I_z denote the velocity, mass and yaw moment of inertia.

Assuming that the tire parameters are updated and constant during one control time step, the prediction model in equation (7) can be represented in discrete-time.

$$\begin{aligned}\mathbf{x}(k+1) &= A_d\mathbf{x}(k) + B_d\mathbf{u}(k)\\ \mathbf{y}(k) &= C\mathbf{x}(k)\end{aligned} \tag{8}$$

where $A_d = I + T_s \cdot A$, $B_d = T_s \cdot B$.

3.3. Estimation of Tire Parameter

In order to consider the nonlinear characteristics of tire in emergency steering, the tire parameters in equation (7) are estimated and updated in the prediction model. While the nonlinear characteristics of tires can be experimentally investigated such as Magic formula (Pacejka and Bakker, 1992), variation of the cornering stiffness is described as extra state variables in this study and their values are estimated based on the following dynamic equation (Lee *et al*., 2012).

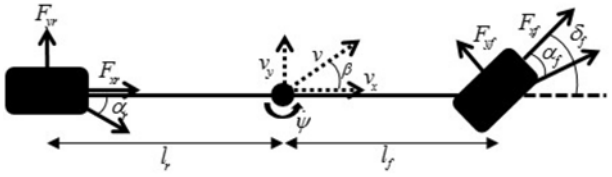

Figure 4. Lateral vehicle dynamics model.

$$\begin{aligned}\dot{\underline{\mathbf{x}}} &= f(\underline{\mathbf{x}}, \mathbf{u})\\ \underline{\mathbf{y}} &= h(\underline{\mathbf{x}}, \mathbf{u})\end{aligned} \tag{9}$$

where

$\underline{\mathbf{x}} = \begin{bmatrix} v_x & v_y & \dot{\psi} & \Delta C_f & \Delta C_r & F_{xf} \end{bmatrix}^T \equiv \begin{bmatrix} \underline{x}_1 & \underline{x}_2 & \underline{x}_3 & \underline{x}_4 & \underline{x}_5 & \underline{x}_6 \end{bmatrix}^T$,

$\underline{\mathbf{y}} = \begin{bmatrix} v_x & \dot{\psi} & a_x & a_y \end{bmatrix}^T$, $\mathbf{u} = \delta_f \equiv u_1$,

$$f(\underline{\mathbf{x}}, \mathbf{u}) = \begin{bmatrix} \underline{x}_2\underline{x}_3 + \dfrac{1}{m}\left\{\underline{x}_6 \cos(u_1) - (C_f + \underline{x}_4)\alpha_f \sin(u_1)\right\} \\ -\underline{x}_1\underline{x}_3 + \dfrac{1}{m}\left\{\underline{x}_6 \sin(u_1) + (C_f + \underline{x}_4)\alpha_f \sin(u_1) + (C_r + \underline{x}_5)\alpha_r\right\} \\ \dfrac{1}{I_z}\left\{l_f \underline{x}_6 \sin(u_1) + l_f (C_f + \underline{x}_4)\alpha_f \cos(u_1) - l_r (C_r + \underline{x}_5)\alpha_r\right\} \\ 0 \\ 0 \\ 0 \end{bmatrix},$$

$$h(\underline{\mathbf{x}}, \mathbf{u}) = \begin{bmatrix} \underline{x}_1 \\ \underline{x}_3 \\ \dfrac{1}{m}\left\{\underline{x}_6 \cos(u_1) - (C_f + \underline{x}_4)\alpha_f \sin(u_1)\right\} \\ \dfrac{1}{m}\left\{\underline{x}_6 \sin(u_1) + (C_f + \underline{x}_4)\alpha_f \sin(u_1) + (C_r + \underline{x}_5)\alpha_r\right\} \end{bmatrix}.$$

In the above equation, front and rear slip angles, α_f and α_r, are calculated based on the measured velocity and the estimated lateral velocity. EKF approach (Grewal, 2011) is applied after equation (9) is discretized into a discrete form.

$$\begin{aligned}\underline{\mathbf{x}}_{k+1} &= \boldsymbol{f}(\underline{\mathbf{x}}_k, \mathbf{u}_k) + w_k\\ \underline{\mathbf{y}}_k &= \boldsymbol{h}(\underline{\mathbf{x}}_k, \mathbf{u}_k) + v_k\end{aligned} \tag{10}$$

The state vector and the error covariance matrix are predicted using equation (11) and the Kalman filter gain is calculated using equation (12).

$$\begin{aligned}\bar{\underline{\mathbf{x}}}_k &= \boldsymbol{f}(\hat{\underline{\mathbf{x}}}_{k-1}, \mathbf{u}_{k-1})\\ \bar{\underline{\Sigma}}_k &= \boldsymbol{\Phi}_{k-1}\underline{\Sigma}_{k-1}{\boldsymbol{\Phi}_{k-1}}^T + \underline{Q}\end{aligned} \tag{11}$$

$$K_k = \bar{\underline{\Sigma}}_k {C_k}^T (C_k \bar{\underline{\Sigma}}_k {C_k}^T + \underline{R})^{-1} \tag{12}$$

where $\underline{Q} = diag\left(\sigma_{w1}^2, \sigma_{w2}^2, \sigma_{w3}^2, \sigma_{w4}^2, \sigma_{w5}^2, \sigma_{w6}^2\right)$,

$\underline{R} = diag\left(\sigma_{v1}^2, \sigma_{v2}^2, \sigma_{v3}^2, \sigma_{v4}^2\right)$.

The superscripts of – and ^ represent the predicted and estimated values, respectively. The Jacobian matrix of $\boldsymbol{\Phi}_k$ and C_k are obtained from the following relations.

$$\Phi_k = \left.\frac{\partial \boldsymbol{f}(\underline{\mathbf{x}},\mathbf{u})}{\partial \underline{\mathbf{x}}}\right|_{\underline{\mathbf{x}}=\hat{\underline{\mathbf{x}}}_{k-1}}, \; C_k = \left.\frac{\partial \boldsymbol{h}(\underline{\mathbf{x}},\mathbf{u})}{\partial \underline{\mathbf{x}}}\right|_{\underline{\mathbf{x}}=\bar{\underline{\mathbf{x}}}_k} \tag{13}$$

Based on the EKF formulation (Grewal, 2011), the estimated state vector and the error covariance are updated.

$$\begin{aligned} \hat{\underline{\mathbf{x}}}_k &= \bar{\underline{\mathbf{x}}}_k + K_k\left(\underline{\mathbf{y}}_k - \boldsymbol{h}(\bar{\underline{\mathbf{x}}}_k)\right) \\ \Sigma_k &= (I - K_k C_k \bar{\Sigma}_k) \end{aligned} \tag{14}$$

Simulations are performed to validate the performance of the designed estimator for the tire parameters. Simulation are conducted on CarSim in connection with MATLAB/Simulink and true value of vehicle motion information is obtained through CarSim. When a sine wave steering input is applied while the vehicle is driving at 100 km/h, maneuvering variables are compared with and without estimated cornering stiffness. As shown in Figure 5, the calculated lateral states such as side-slip angle and yaw rate follow the actual values well with the estimated cornering stiffness at the front and rear wheels.

4. STEERING CONTROLLER DESIGN FOR COLLISION AVOIDANCE

Steering control input should be obtained by considering the steering maneuverability, the capacity of the steering actuator and the safe avoidance region. In the controller design through MPC (Model Predictive Control) (Camacho and Alba, 2013), the lateral dynamics in equation (8) is used as a prediction model and the cost function is formulated based on the tracking error and the input size.

4.1. Cost Function of the MPC Controller

The cost function is defined as follows and is minimized for selecting the steering control input.

$$J_k = \sum_{i=0}^{N_p-1}\left(\left\|\mathbf{y}(k+i+1|k) - \mathbf{y}_{ref}(k+i+1|k)\right\|_Q^2 + \left\|\Delta\mathbf{u}(k+i|k)\right\|_R^2\right) \tag{15}$$

where $\mathbf{y}_{ref}$ and $\Delta\mathbf{u}$ denote the target output and the control input rate, respectively. The target output consists of the desired lateral distance, y_{target}, and the desired heading angle, ψ_{target}. As illustrated in Figure 6, if the straight motion of the host vehicle can induce collision, the target output is generated to change the lane for collision avoidance. The time margin to avoid the collision with the surrounding vehicle is described by TTC (Time To Collision) and the number of time steps for possible collision can be calculated.

$$\begin{aligned} TTC &= \frac{d}{v_{x,rel}} \\ N_{TTC} &\le \frac{TTC}{T_s} < N_{TTC} + 1 \end{aligned} \tag{16}$$

where d is the relative distance to the surrounding vehicle and N_{TTC} is the number of time steps for possible collision.

Then, the target lateral distance, y_{target}, is determined to follow the avoidance path and its value is updated at every control step.

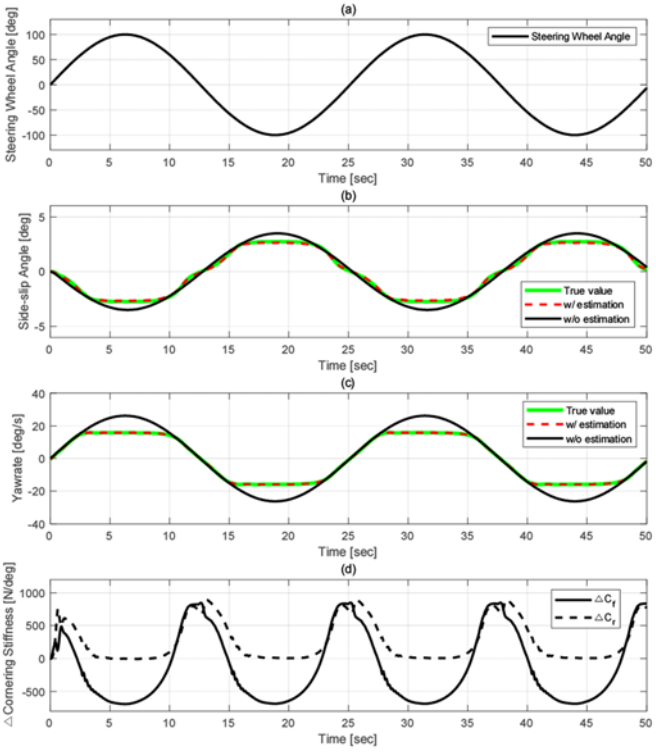

Figure 5. Estimation results: (a) steering wheel angle, (b) side-slip angle, (c) yaw rate and (d) variation of cornering stiffness.

$$y_{target} = y_{N_{TTC}}^{obj} \pm \left(\frac{w_{ego} + w_{obj}}{2} + y_{margin}\right) \tag{17}$$

where $y_{N_{TTC}}^{obj}$ is the predicted lateral position of the surrounding vehicle after N_{TTC} steps. w_{ego} and w_{obj} are the width of the host and surrounding vehicle. y_{margin} denotes tolerance of the avoidance maneuvering. ± sign in equation (17) represents the avoidance maneuvering to the right or left side of the surrounding vehicle. Also, in order to follow the lane during the avoidance, ψ_{target} is updated at every step to the angle between the directions of the host vehicle and the lane as illustrated in Figure 6.

4.2. Constraints of the MPC Controller

One of the advantages for MPC formulation (Camacho and Alba, 2013) is that it can determine optimal input considering the constraints such as boundaries, input size, etc. In this study, two constraints are considered such as safe avoidance region and actuator capacity. In order to define the constraints of safe avoidance region, future states such as heading angle of the host vehicle are required. However, the future states can be obtained through optimization with defined constraints. Assuming the following sinusoidal path in Figure 7 during the emergency lane change:

$$y(x) = y_e\left[\frac{x}{x_e} - \frac{1}{2\pi}\sin\left(\frac{2\pi x}{x_e}\right)\right] \tag{18}$$

The maximum heading angle can be expressed as follows (Sledge and Marshek, 1997) and its value depends on the allowable lateral acceleration and speed.

$$\psi_{\max}\left(v_x^{ego}\right)=\tan^{-1}\left(y'\left(\frac{x_e}{2}\right)\right) \tag{19}$$

where $x_e = C_x v_x^{ego}\sqrt{\frac{y_e}{a_y}}$.

4.2.1. Safe Avoidance Region

The avoidance path from the MPC controller should be contained inside the safe region which is expressed as the lateral distance range along the predicted path. The upper and lower limit of the range is predicted at every control step considering the trajectory of the surrounding vehicles and road boundary.

$$\begin{aligned} &y_{\min}\left(k+i|k\right)\le y\left(k+i|k\right)\le y_{\max}\left(k+i|k\right)\\ &i=1,\cdots,N_p \end{aligned} \tag{20}$$

where $y_{\min}(k+i|k)$ and $y_{\max}(k+i|k)$ are the minimum and maximum lateral distances predicted for i-steps ahead, respectively.

The limit of the lateral distance is defined as the constraint, $y_{con} = [y_{\min}\ y_{\max}]^T$, and its description is expressed in equation (21) and (22). As illustrated in Figures 8 (b) and 8 (c), the lateral motion in collision avoidance is allowed up to the right or left lane unless there exist overlap between the predicted ellipses of the host vehicle and surrounding vehicles. If their x-coordinate values are identical at the same time, the ellipse of the host vehicle is moved laterally and is rotated either for the lane-keeping or for the evasive maneuvering with the maximum heading angle.

$$\begin{aligned} &\text{for } i=1,\cdots,N_{TTC}\\ &\quad \textit{if } \mathrm{E}_{X,k+i}\cap\mathrm{O}_{X,k+i}=\phi,\\ &\qquad \mathbf{y}_{con}\left(k+i|k\right)=\left[y_{\min}^{lane}(k+i|k)\ \ y_{\max}^{lane}(k+i|k)\right]^T\\ &\quad \textit{else},\\ &\qquad \mathbf{y}_{con}\left(k+i|k\right)=\left[y_{CA}(k+i|k)\ \ y_{\max}^{lane}(k+i|k)\right]^T\\ &\qquad\qquad \textit{or}\\ &\qquad \mathbf{y}_{con}\left(k+i|k\right)=\left[y_{\min}^{lane}(k+i|k)\ \ y_{CA}(k+i|k)\right]^T \end{aligned} \tag{21}$$

$$\begin{aligned} &\text{for } i=N_{TTC}+1,\cdots,N_p\\ &\quad \mathbf{y}_{con}\left(k+i|k\right)=\left[y_{\min}^{lane}(k+i|k)\ \ y_{\max}^{lane}(k+i|k)\right]^T \end{aligned} \tag{22}$$

where $y_{\min}^{lane}(k+i|k)$, $y_{\max}^{lane}(k+i|k)$, and $y_{CA}(k+i|k)$ are lateral distances to the right lane, left lane and avoidance boundary predicted for i-steps ahead, respectively. $\mathrm{E}_{x,k+i}$ and $\mathrm{O}_{x,k+i}$ represent sets of local x-coordinates of the host vehicle ellipse and surrounding vehicle ellipse predicted for i-steps ahead, respectively.

4.2.2. Actuator Capacity Constraint

The capacity of the steering actuator should be considered for the MPC formulation and, thus, the physical limits for the steering angle and angular speed are set as the constraints.

$$\begin{aligned} &\mathrm{u}_{\min}\le \mathrm{u}\left(k+i+1\,|\,k\right)\le \mathrm{u}_{\max}\\ &\Delta\mathrm{u}_{\min}\le \Delta\mathrm{u}\left(k+i\,|\,k\right)\le \Delta\mathrm{u}_{\max}\\ &i=0,\cdots,N_p-1 \end{aligned} \tag{23}$$

where $\mathrm{u}_{\min}$ and $\mathrm{u}_{\max}$ are minimum and maximum steering angle, respectively. $\Delta\mathrm{u}_{\min}$ and $\Delta\mathrm{u}_{\max}$ are minimum and maximum steering angular speed, respectively.

4.3. MPC Formulation

In order to convert the optimization problem in equation (15) into a constrained standard quadratic problem, the prediction model in equation (8) is transformed into an IIO (Increment-Input-Output) model.

$$\bar{\mathbf{x}}\left(k+1\right)=A_a\bar{\mathbf{x}}\left(k\right)+B_a\Delta\mathbf{u}\left(k\right) \tag{24}$$

where

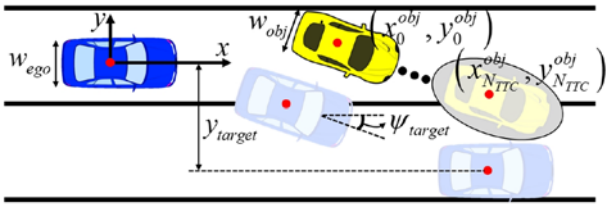

Figure 6. Target position of the host vehicle during avoidance.

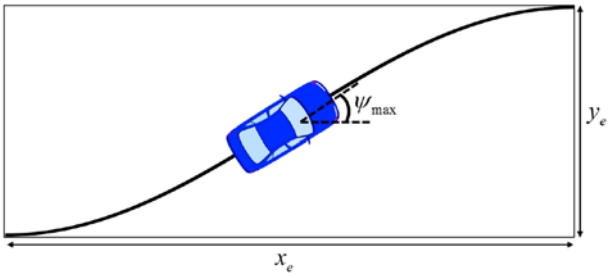

Figure 7. Sinusoidal path during lane change.

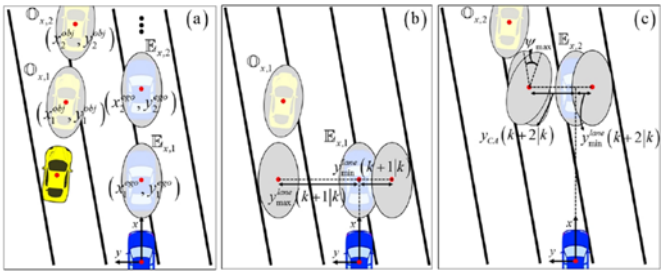

Figure 8. Constraints of lateral distance for safe avoidance region.

$$\bar{\mathbf{x}}(k)=\begin{bmatrix}\mathbf{x}(k)\\ \mathbf{u}(k-1)\end{bmatrix},\ A_a=\begin{bmatrix}A_d & B_d\\ \phi & \mathrm{I}\end{bmatrix},$$

$$B_a=\begin{bmatrix}B_d\\ \mathrm{I}\end{bmatrix},\ \Delta\mathbf{u}(k)=\mathbf{u}(k)-\mathbf{u}(k-1).$$

The output is predicted up to the prediction horizon by using the IIO model.

$$\mathbf{Y}=F\bar{\mathbf{x}}(k)+\Phi\Delta\mathbf{U} \tag{25}$$

where $\mathbf{Y}=\begin{bmatrix}\mathbf{y}(k+1|k)\\ \mathbf{y}(k+2|k)\\ \vdots\\ \mathbf{y}(k+N_p|k)\end{bmatrix},\ F=\begin{bmatrix}CA_a\\ CA_a^2\\ \vdots\\ CA_a^{Np}\end{bmatrix},$

$$\Phi=\begin{bmatrix}CB_a & 0 & 0 & 0\\ CA_aB_a & CB_a & 0 & 0\\ \vdots & \vdots & \ddots & 0\\ CA_a^{Np-1}B_a & CA_a^{Np-2}B_a & \cdots & CA_a^{Np-Np}B_a\end{bmatrix},$$

$$\Delta\mathbf{U}=\begin{bmatrix}\Delta\mathrm{u}(k|k)\\ \Delta\mathrm{u}(k+1|k)\\ \vdots\\ \Delta\mathrm{u}(k+N_p-1|k)\end{bmatrix}.$$

By using equation (25) and matrix manipulations (Camacho and Alba, 2013), the cost function of equation (15) is expressed into the following form.

$$\begin{aligned}J&=\left(\mathbf{Y}-\mathbf{Y}_{ref}\right)^T Q\left(\mathbf{Y}-\mathbf{Y}_{ref}\right)^T+\Delta\mathbf{U}^T R\Delta\mathbf{U}\\ &=\frac{1}{2}\Delta\mathbf{U}^T H\Delta\mathbf{U}+\Delta\mathbf{U}^T f+\text{const.}\end{aligned} \tag{26}$$

where $H=\Phi^T Q\Phi+R,\ f=\Phi^T Q\left(F\bar{\mathbf{x}}(k)-\mathbf{Y}_{ref}\right),$

$$\mathbf{Y}_{ref}=\begin{bmatrix}\mathbf{y}_{ref}(k+1|k)\\ \mathbf{y}_{ref}(k+2|k)\\ \vdots\\ \mathbf{y}_{ref}(k+N_p|k)\end{bmatrix}.$$

The constraints in section 3.2 can be expressed into the following form for the constrained standard quadratic problem:

$$\begin{bmatrix}M_1\\ M_2\\ M_3\end{bmatrix}\Delta\mathbf{U}\le\begin{bmatrix}N_1\\ N_2\\ N_3\end{bmatrix} \tag{27}$$

where $M_1=\begin{bmatrix}-C_2\\ C_2\end{bmatrix},\ N_1=\begin{bmatrix}-\mathbf{U}_{\min}+C_1\mathbf{u}(k-1)\\ \mathbf{U}_{\max}-C_1\mathbf{u}(k-1)\end{bmatrix},\ M_2=\begin{bmatrix}-I\\ I\end{bmatrix},$

$$N_2=\begin{bmatrix}-\Delta\mathbf{U}_{\min}\\ \Delta\mathbf{U}_{\max}\end{bmatrix},\ M_3=\begin{bmatrix}-\Phi\\ \Phi\end{bmatrix},\ N_3=\begin{bmatrix}-\mathbf{Y}_{\min}+F\bar{\mathbf{x}}(k)\\ \mathbf{Y}_{\max}-F\bar{\mathbf{x}}(k)\end{bmatrix},$$

$$C_1=\begin{bmatrix}I\\ I\\ \vdots\\ I\end{bmatrix},\ C_2=\begin{bmatrix}I & 0 & 0 & 0\\ I & I & 0 & 0\\ \vdots & \vdots & \ddots & 0\\ I & I & \cdots & I\end{bmatrix}.$$

Based on equation (26) and (27), the optimal input for $\Delta\mathbf{U}$ is determined at every step using QP solver (Camacho and Alba, 2013).

5. ACTIVATION TIME FOR COLLISION AVOIDANCE CONTROL

When the collision is imminent and the driver does not respond to the collision warning, active control is attempted by braking first to avoid or mitigate collision. In this AEB (Autonomous Emergency Braking) case, the activation time can be calculated as the TTC (Time To Collision) assuming that the longitudinal deceleration of the host vehicle is constant (Eckert *et al*., 2011).

$$TTC_{AEB}=\frac{v_{x,rel}}{2a_{x,AEB}} \tag{28}$$

where TTC_{AEB} is the TTC for AEB activation and $a_{x,AEB}$ is the preset longitudinal deceleration in AEB operation. Because the deceleration of a vehicle is limited, the last point to avoid collision by braking can be described as the following TTC:

$$TTC_{brake}=\frac{v_{x,rel}}{2a_{x,brake}} \tag{29}$$

where TTC_{brake} is the smallest TTC for AEB activation. $a_{x,brake}$ is the maximum longitudinal deceleration in braking and satisfies $|a_{x,brake}| > |a_{x,AEB}|$ and, thus, $TTC_{brake} < TTC_{AEB}$. Because the driver could apply the maximum braking to avoid collision, the active steering control such as AES (Autonomous Emergency Steering) needs to wait up to this point. Besides, the AES system of the host vehicle should be applied only when its steering maneuvering does not cause any accident with other surrounding vehicles or road structures.

The AES system should include not only the avoidance path by steering, but also the recovering path by reverse steering to stabilize inside the lane. The last point to avoid collision by AES can be described as the following TTC by assuming that the lateral acceleration is constant during the avoidance path:

$$TTC_{steer}=\min_{l,r}\left(\sqrt{\frac{2|y_{target}|}{a_{y,\max}}}\right) \tag{30}$$

where TTC_{steer} is the smallest TTC for AES activation, $a_{y,\max}$ is the maximum lateral acceleration in AES operation and y_{target} is the target lateral position for lane change. The minimum value in equation (30) represents smaller TTC between the right and left side maneuvering to the obstacle. Based on equations (29) and (30), the intervenable time for the AES can

be defined as the following set.

$$TTC_{AES} \equiv \{TTC | TTC_{steer} < TTC < TTC_{brake}\} \tag{31}$$

Furthermore, the intervention with the AES system is set to occur only when it is needed. In other words, the AES system waits for the last moment when the steering avoidance is still possible by the driver. In this study, the AES system is activated when the expected lateral acceleration of the avoidance path is greater than a threshold value under which the collision can be avoided by the driver's steering. Based on the optimal path designed by the MPC in Section 3, the lateral acceleration can be calculated as follows.

$$a_y(k+i|k) = v_x^{ego}\left(\frac{\beta(k+i|k)-\beta(k+i-1|k)}{T_s}+\dot{\psi}(k+i|k)\right) \quad for\ i=1,\cdots,N_p \tag{32}$$

where $a_y(k+i|k)$, $\beta(k+i|k)$ and $\dot{\psi}(k+i|k)$ are lateral acceleration, side-slip angle and yaw rate predicted for i-steps ahead, respectively.

From equation (32), the maximum lateral acceleration generated during the entire avoidance trajectory is determined at every control step.

$$a_{y,\max}(k) = \max_{i=1:Np}\left(\left|a_y(k+i|k)\right|\right) \tag{33}$$

Then, the activation time of the AES can be described by the following rule considering equations (31) and (33).

$$TTC_{AES} = \begin{cases} \text{no activation} & \text{if } TTC(k) \notin TTC_{AES} \\ \text{no activation} & \text{if } TTC(k) \in TTC_{AES} \text{ and } a_{y,\max}(k) < a_{y,th} \\ TTC(k) & \text{if } TTC(k) \in TTC_{AES} \text{ and } a_{y,\max}(k) \geq a_{y,th} \end{cases} \tag{34}$$

where $TTC(k)$ is the time to collision calculated at the current time and $a_{y,th}$ is the threshold value for the lateral acceleration.

6. SIMULATION RESULTS

In order to verify the proposed collision avoidance system, two scenarios are considered in simulations which consist of avoiding a slow vehicle within the same lane and avoiding a cut-in vehicle in front of the host vehicle. The reference acceleration values are given in Table 1 for the emergency collision avoidance and their size can be adjusted depending on the degree of intervention. The parameter values for the vehicle and MPC formulation are listed in Table 2.

Table 1. Reference accelerations for calculating TTC indices.

Symbol	Description	Value [unit]
$a_{x,\ AEB}$	Reference deceleration for TTC_{AEB}	9 [m/s^2]
$a_{x,\ brake}$	Reference deceleration for TTC_{brake}	10 [m/s^2]
$a_{y,\ steer}$	Reference acceleration for TTC_{steer}	±8.5 [m/s^2]
$a_{y,\ th}$	Threshold of lateral acceleration	7 [m/s^2]

Table 2. Simulation parameters.

Symbol	Description	Value [unit]
T_s	Sampling time	0.05 [s]
N_p	Prediction horizon	50
u_{min}, u_{max}	Input constraints	-500 [deg], 500 [deg]
Δu_{min}, Δu_{max}	Input rate constraints	-600 [deg/s], 600 [deg/s]
m	Total vehicle mass	1830 [kg]
I_z	Yaw moment of inertia	3234 [kg·m^2]
l_f	Distance from c.g. to front wheels	1.4 [m]
l_r	Distance from c.g. to rear wheels	1.65 [m]

6.1. Scenario 1: Slow Vehicle In Front

In this scenario, the host vehicle is approaching the lead vehicle in the same lane for different relative speed and overlap percentage. The overlap percentage represents the expected percentage of the width of the host vehicle in contact during collision. The potential rear-end collision induces the AEB system activated from equation (28). After 0.1 s subsequent to the AEB application, the lead vehicle decelerates with 1.8 m/s^2 and TTC values for the various cases are listed in Table 3. It should be noted that braking is always considered first as the primary option and the evasive steering with the AES is activated only after the host vehicle passes TTC_{brake} point with equation (31).

The first group with three non-shaded elements in Table 3 are almost identical in that they reach TTC_{brake} after the AEB was applied and it is too late to activate the AES because TTC_{brake} is smaller than TTC_{steer}. Therefore, the host vehicle

Table 3. TTC results of the first scenario.

Overlap % / Init. Rel. Vel	50 %				100 %			
	TTC_{AEB}	TTC_{brake}	TTC_{AES}	TTC_{steer}	TTC_{AEB}	TTC_{brake}	TTC_{AES}	TTC_{steer}
40 km/h	0.68 s	0.53 s	-	0.66 s	0.68 s	0.53 s	-	0.80 s
60 km/h	0.92 s	0.68 s	0.68 s	0.67 s	0.92 s	0.68 s	-	0.81 s
80 km/h	1.27 s	1.00 s	0.78 s	0.67 s	1.27 s	1.00 s	1.00 s	0.68 s

maintains the maximum braking to mitigate damage in unavoidable collision. The second group with three shaded elements in Table 3 demonstrates the AES activation where collision avoidance by braking is judged impossible at TTC_{brake}, but, collision avoidance by steering is still possible because the AES activation condition in equation (34) is satisfied. Even if TTC_{steer} values are very close for the two cases of 80 km/h speed, the activation time of the AES are different because the AES requires less time to avoid collision with smaller overlap percentage.

For the case of 80 km/h relative speed and 50 % overlap percentage, Figure 9 illustrates how the AEB and AES are activated depending on TTC values and the predicted maximum lateral acceleration. The AEB is activated first at 1.27 s TTC and the host vehicle soon reaches the last point to brake, TTC_{brake}. Fortunately, the AES can be activated to avoid the collision at 0.78 s TTC by satisfying the condition of equation (34). During this collision avoidance maneuvering, vehicles states are plotted in Figure 10 such as lateral acceleration, speed and steering angle. Figure 11 (a) shows the predicted paths of the lead and the host vehicles when TTC is equal to TTC_{AES}. The actual avoidance path of the host vehicle is shown with its predicted trajectory in Figure 11 (b). In Figure 11, the black and blue filled ellipses represent the current locations of the lead and host vehicles, respectively. The empty ellipse in the Figure 11 corresponds to a predicted location at every 0.25 s even though the prediction period is actually 0.05 s. The red dotted lines indicate the boundary of the safe avoidance region and the determined avoidance trajectory of the host vehicle lies inside this region.

6.2. Scenario 2: Cut-in Vehicle In Front

In this scenario, the slow vehicle on the left lane suddenly executes cut-in motion in front of the host vehicle. With different relative velocity and cut-in distance, TTC values for the various cases are listed in Table 4. $TTC_{cut\text{-}in}$ represents the initial TTC value to the cut-in vehicle and corresponds to the cut-in distance. Again, it should be noted that braking is always considered first as the primary option and the evasive steering with the AES is activated only after the host vehicle passes TTC_{brake} point with equation (31).

The first group with two non-shaded elements in Table 4 shows that the AEB is activated first because collision overlap is expected between the predicted trajectories of the host and cut-in vehicles. Because the distance to the cut-in vehicle is far

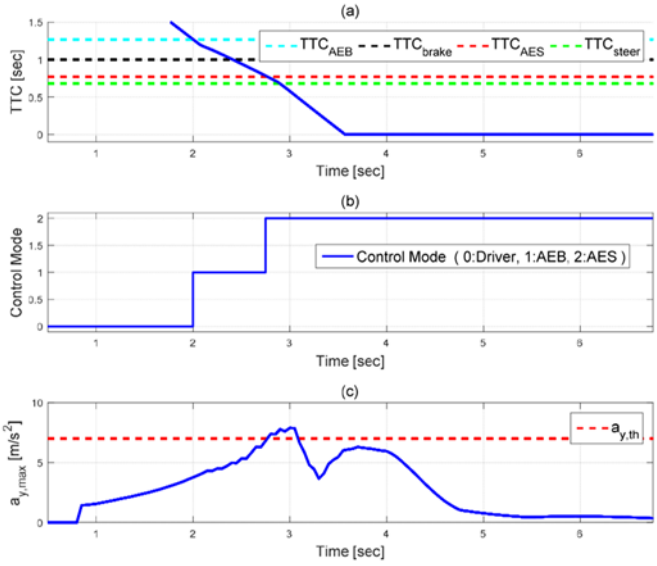

Figure 9. AEB and AES activation results: (a) TTC, (b) control mode and (c) predicted maximum a_y.

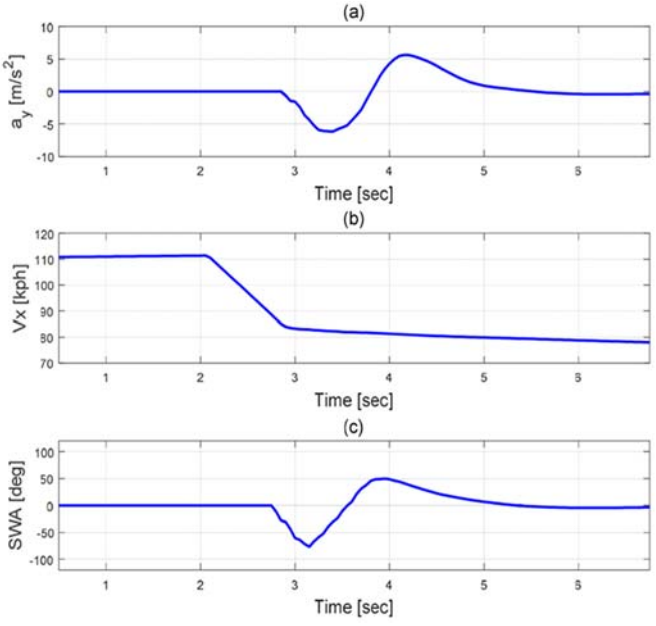

Figure 10. Vehicles states: (a) lateral acceleration, (b) longitudinal velocity and (c) steering wheel angle.

Table 4. TTC results of the second scenario

Init. Rel. Vel \ $TTC_{cut\text{-}in}$	1.5 s				1 s			
	TTC_{AEB}	TTC_{brake}	TTC_{AES}	TTC_{steer}	TTC_{AEB}	TTC_{brake}	TTC_{AES}	TTC_{steer}
40 km/h	0.72 s	-	-	0.92 s	0.68 s	0.58 s	-	0.70 s
60 km/h	0.97 s	-	-	0.94 s	0.95 s	0.80 s	0.80 s	0.68 s
80 km/h	1.29 s	1.13 s	1.13 s	0.95 s	1.27 s	1.11 s	0.80 s	0.71 s

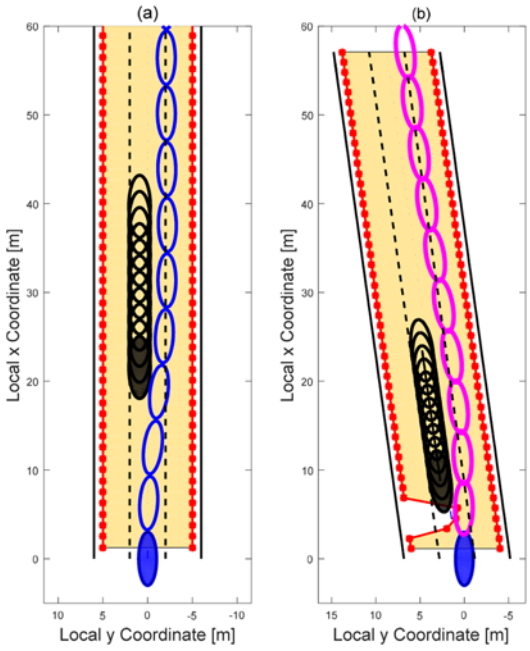

Figure 11. Avoidance trajectory: (a) when $TTC = TTC_{ABS}$ and (b) during collision avoidance.

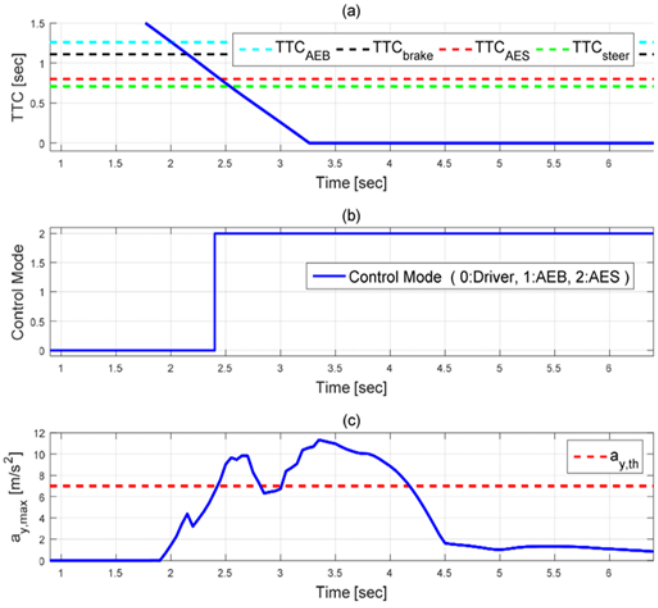

Figure 12. AES activation results: (a) TTC, (b) control mode and (c) predicted maximum a_y.

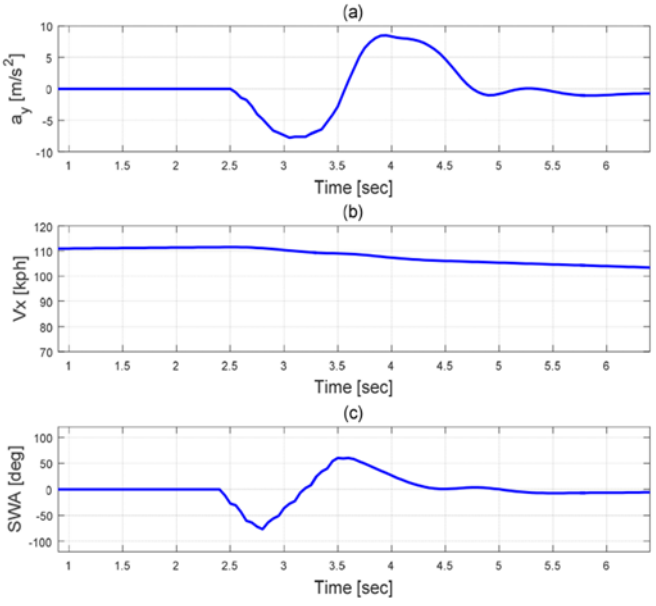

Figure 13. Vehicles states in AES: (a) lateral acceleration, (b) longitudinal velocity and (c) steering wheel angle.

enough, braking only inside the ego lane can prevent the collision against the cut-in vehicle. The second group with one lightly-shaded element in Table 4 shows the opposite example that the AEB is not activated until small TTC because there exists no intersection between the predicted trajectories of the host and cut-in vehicles. However, when the nearby vehicle on the left side suddenly attempts cut-in into the ego lane, TTC_{AEB} and TTC_{brake} are confronted right away for the host vehicle. It is too late to avoid collision either by braking or steering, so just full braking is applied to reduce collision damage. The third group with three shaded elements in Table 4 is similar with the second group in that the AEB is not activated because collision is not expected at the moment between the predicted trajectories of the host and cut-in vehicles. When the left vehicle suddenly attempts cut-in into the ego lane, collision avoidance by braking is judged impossible at TTC_{brake}, but, collision avoidance by steering is still possible because the AES activation condition in equation (34) is satisfied. The third group demonstrates successful collision avoidance by steering when the collision cannot be avoided by braking.

For the case of 80 km/h relative speed and initial $TTC_{cut\text{-}in}$ of 1 s, the AES activation with varying TTC values and the predicted maximum lateral acceleration are plotted in Figure 12. Even if the host vehicle encounters TTC_{AEB} and TTC_{brake}, the AEB is not activated because there exists no intersection between the predicted trajectories of the host and cut-in vehicles. When the cut-in vehicle invades the ego lane, TTC_{AEB} and TTC_{brake} have been passed, but fortunately there is still time to steer the vehicle to avoid the collision. Figure 13 shows the vehicle states in the AES operation where not only the collision avoidance, but also the lane keeping are achieved. Using MATLAB R2019a on Intel Core i7-9700K 3.60GHz processor with 16 GB RAM, the average time for one whole iteration of the algorithm takes 0.0025 s. Thus, the proposed control system can achieve the real-time performance.

7. CONCLUSION

In this paper, an AES system is proposed to avoid the collision in situations where collision avoidance is impossible with the AEB. The predicted trajectories of the surrounding vehicles as well as the host vehicle are utilized to judge the collision and a safe avoidance region is determined considering the road shape. In order to improve the trajectory accuracy of the host vehicle, the nonlinear cornering stiffness of tires is estimated and updated in the prediction model. The MPC framework is applied to obtain the optimal steering input based on the cost function with the constraints of the safe avoidance region and the actuator capacity. The time margins by the AEB and the AES systems are considered for collision avoidance and their intervention rules are designed such that the AES system should be applied only when it is effective. In particular, for the AES activation, not only the TTC index, but also the maximum lateral acceleration index is considered because the AES function includes both the avoidance and the lane keeping paths. In order to verify the proposed AES system, simulations are conducted and compared with the AEB system for various collision scenarios. As illustrated in the simulation results for severe cases such as abrupt cut-in vehicles, collision is unavoidable either by AEB or AES system. However, there exist several cases where the collision can be avoided effectively by the proposed AES system even after it is judged that the collision is unavoidable by the AEB systems. It is demonstrated that the proposed algorithm of integrating the AEB and the AES systems can improve the collision avoidance capability compared with the AEB alone in ADAS applications.

ACKNOWLEDGEMENT–This work was supported by the Industrial Strategic Technology Development Program(10079730, Development and Evaluation of Automated Driving Systems for Motorway and City Road) funded By the Ministry of Trade, Industry & Energy(MOTIE, Korea).

REFERENCES

Berthelot, A., Tamke, A., Dang, T. and Breuel, G. (2012). A novel approach for the probabilistic computation of time-to-collision. *IEEE Intelligent Vehicles Symp*. Alcalá de Henares, Spain.

Camacho, E. F. and Alba, C. B. (2013). *Model predictive control*. Springer Science & Business Media. Berlin, Germany.

Carvalho, A., Gao, Y., Lefevre, S. and Borrelli, F. (2014). Stochastic predictive control of autonomous vehicles in uncertain environments. *12th Int. S. Advanced Vehicle Control (AVEC'14)*. Tokyo, Japan.

Eckert, A., Hartmann, B., Sevenich, M. and Rieth, P. E. (2011). Emergency steer & brake assist: a systematic approach for system integration of two complementary driver assistance systems. *Proc. 22nd Int. Technical Conf. Enhanced Safety of Vehicles*. Washington DC, USA.

Erlien, S. M., Fujita, S. and Gerdes, J. C. (2016). Shared steering control using safe envelopes for obstacle avoidance and vehicle stability. *IEEE Trans. Intelligent Transportation Systems* **17**, **2**, 441–451.

Europ NCAP (2015). 2020 Roadmap, Revision 1. https://cdn.euroncap.com/media/16472/euro-ncap-2020-roadmap-rev1-march-2015.pdf

Falcone, P., Borrelli, F., Asgari, J., Tseng, H. E. and Hrovat, D. (2007). Predictive active steering control for autonomous vehicle systems. *IEEE Trans. Control Systems Technology* **15**, **3**, 566–580.

Goodrich, J. (2013). Driving miss daisy: an autonomous chauffeur system. *Houston Law Review* **51**, **1**, 265–296.

Grewal, M. S. (2011). *Kalman filtering*. Int. Encyclopedia of Statistical Science: Springer, 705–708.

Keller, M., Haß, C., Seewald, A. and Bertram, T. (2015). A model predictive approach to emergency maneuvers in critical traffic situations. *IEEE Conf. Intelligent Transportation Systems (ITSC),* 369–374.

Kim, H., Cho, J., Kim, D. and Huh, K. (2017). Intervention minimized semi-autonomous control using decoupled model predictive control. *IEEE Intelligent Vehicles Symp*., 618–623.

Lee, D., Kim, I. and Huh, K. (2012). Tire lateral force estimation system using nonlinear Kalman filter. *Trans. Korean Society of Automotive Engineers* **20**, **6**, 126–131.

Lee, D., Kim, S., Kim, C. and Huh, K. (2014). Development of an autonomous braking system using the predicted stopping distance. *Int. J. Automotive Technology* **15**, **2**, 341–346.

Lefèvre, S., Vasquez, D. and Laugier, C. (2014). A survey on motion prediction and risk assessment for intelligent vehicles. *Robomech J.* **1**, **1**, 1–14.

Liu, C., Lee, S., Varnhagen, S. and Tseng, H. E. (2017). Path planning for autonomous vehicles using model predictive control. *IEEE Intelligent Vehicles Symp*., 174–179.

Pacejka, H. B. and Bakker, E. (1992). The magic formula tyre model. *Vehicle System Dynamics*, **21**, 1–18.

Ribeiro M. I. (2004). Gaussian probability density functions: Properties and error characterization. *Institute for Systems and Robotics*. Lisboa, Portugal.

Schmidt, C., Oechsle, F. and Branz, W. (2006). Research on trajectory planning in emergency situations with multiple objects. *IEEE Conf. Intelligent Transportation Systems (ITSC)*, 988–992.

Schram, R., Williams, A. and van Ratingen, M. (2013). Implementation of Autonomous Emergency Braking (AEB), the next step in Euro NCAP'S safety assessment. *ESV*, Seoul.

Shah, J. and Benmimoun, M. (2015). Driver perceived threat and behavior in rear end collision avoidance situations. *SAE Paper No*. 2015-01-1414.

Sledge, N. H. and Marshek, K. M. (1997). Comparison of ideal vehicle lane-change trajectories. *SAE Trans.* 2004–2027.

Söntges, S. and Althoff, M. (2015). Determining the nonexistence of evasive trajectories for collision avoidance systems. *IEEE Conf. Intelligent Transportation Systems (ITSC)*, 956–961.

Tamke, A., Dang, T. and Breuel, G. (2011). A flexible method for criticality assessment in driver assistance systems. *IEEE Intelligent Vehicles Symp*., 697–702.

Werling, M. and Liccardo, D. (2012). Automatic collision avoidance using model-predictive online optimization. *IEEE Conf. Decision and Control (CDC)*, 6309–6314.

Yoon, Y., Shin, J., Kim, H. J., Park, Y. and Sastry, S. (2009). Model-predictive active steering and obstacle avoidance for autonomous ground vehicles. *Control Engineering Practice* **17**, **7**, 741–750.